

# Change of shell structure and magnetic moments of odd- $N$ deformed nuclei towards neutron drip line

Ikuko Hamamoto<sup>1,2</sup>

<sup>1</sup> *Division of Mathematical Physics,*

*Lund Institute of Technology at the University of Lund,*

*Lund, Sweden*

<sup>2</sup> *The Niels Bohr Institute,*

*Blegdamsvej 17, Copenhagen Ø,*

*DK-2100, Denmark*

## Abstract

Examples of the change of neutron shell-structure in both weakly-bound and resonant neutron one-particle levels in nuclei towards the neutron drip line are exhibited. It is shown that the shell-structure change due to the weak binding may lead to the deformation of those nuclei with the neutron numbers  $N \approx 8, 20, 28$  and  $40$ , which are known to be magic numbers in stable nuclei. Nuclei in the "island of inversion" are most easily and in a simple manner understood in terms of deformation. As an example of spectroscopic properties other than single-particle energies, magnetic moments of some weakly-bound possibly deformed odd- $N$  nuclei with neutron numbers close to those traditional magic numbers are given, which are calculated using the wave function of the last odd particle in deformed Woods-Saxon potentials.

PACS numbers:

## I. INTRODUCTION

Some neutron-rich nuclei towards the neutron drip line, which have the neutron numbers  $N \approx 8$  and 20, are now widely recognized to be deformed and often called nuclei in the "island of inversion" [1–3]. In this paper the change of shell structure in weakly-bound and one-particle resonant neutron levels coming from a unique behaviour of small- $\ell$  neutron levels compared with large- $\ell$  levels is exhibited. The behaviour comes from the strong  $\ell$ -dependence of the heights of centrifugal barrier, which are proportional to  $\ell(\ell+1)/R_b^2$  where  $R_b$  is slightly larger than the nuclear radius. The centrifugal barrier is absent for  $s$  neutrons which can thus freely extend to the outside of nuclei as the binding energy approaches zero. Consequently, the energy of weakly-bound  $s$  neutron levels is relatively insensitive to the strength of the potential. In contrast, large- $\ell$  neutrons are confined to the inside of the potential and, thus, sensitive to the strength of the potential. The barrier becomes increasingly higher both for larger  $\ell$  neutrons and for smaller nuclei. As an example, in figure 1 we sketch the relative energies of three one-neutron levels in the  $sd$  shell depending on binding energies. The figure illustrates how the levels with smaller  $\ell$ -values shift downwards relative to those with larger  $\ell$ -values, as the potential strength becomes weaker. The cases of the strongly bound (such as by 30 MeV) levels and those bound by about 10 MeV (approximately equal to the Fermi level of stable  $sd$  shell nuclei) can be found from figure 2-30 of [4], while the level order of very weakly bound or one-particle resonant neutrons can be found for example in figure 1 of [5, 6]. The level scheme being bound by about 10 MeV is similar to that of the conventional modified-oscillator potential plus a spin-orbit potential. This similarity is accidental. Namely, this never means that "the one-particle level scheme of weakly-bound neutrons becomes similar to that of the harmonic oscillator potential (plus a spin-orbit potential)", which is unfortunately often stated in some publications. Indeed, the harmonic oscillator potential has no surface and, consequently, using the potential it is impossible to express some phenomena which are unique in weakly-bound particles.

The similar change of the relative level order and the shell structure, which is sketched in figure 1 for the  $sd$  shell, occurs for other shells. For example, in the  $pf$  shell the  $p_{3/2}$  and  $p_{1/2}$  levels are lowered relative to the  $1f_{7/2}$  and  $1f_{5/2}$  levels as the potential becomes weaker or the binding energies become smaller, since the centrifugal barrier for  $\ell=1$  neutrons is six times lower than that for  $\ell=3$  neutrons. This change of the shell structure can lead to the

deformed ground state of some nuclei with the traditional magic number for neutrons. See examples in section 3.

Whether a given nucleus with weakly-bound neutrons will deform or not depends, of course, also on the proton number, since some proton number may definitely favor spherical shape. For example, the proton number  $Z=8$ , oxygen isotope, has been known to prefer spherical shape. Nevertheless, it was recently reported [7] that the unbound nucleus  ${}^8_8\text{O}_4$  outside the proton drip line is deformed in the way similar to its mirror nucleus  ${}^{12}_4\text{Be}_8$ .

It is important to notice that the notion of one-particle states in deformed nuclei can be much more widely, in a good approximation, applicable than that in spherical nuclei. This is because in the deformed mean field the major part of the long-range two-body interaction in the spherical mean field is already taken into account in the mean field. Thus, the spectroscopy of deformed nuclei is often much simpler than that of spherical (vibrating) nuclei. For example, we note that the analysis of observed spectroscopic properties of low-lying states in light mirror nuclei,  ${}^{25}_{12}\text{Mg}_{13}$  and  ${}^{25}_{13}\text{Al}_{12}$ , in terms of one-particle motion in deformed (Nilsson) potential is very successful [8]. As seen in those examples, the numerical results of the intrinsic configurations, which are obtained in the present work for the ground state of nuclei with the neutron number of  $N_{magic} \pm 1$ , can be equally applicable to the low-lying excited states (or isomeric states) of the neighboring nuclei.

As the one-particle energy  $\varepsilon_\Omega < 0$  approaches zero in a deformed potential, the probability of  $\ell = 0$  component in the wave function approaches unity in all  $\Omega^\pi=1/2^+$  bound neutron orbits. However, the energy, at which the  $s$ -dominance shows up, depends on both deformation and individual orbits. On the other hand, in the case of  $\Omega^\pi=1/2^-$  and  $\Omega^\pi=3/2^-$  the  $p$ -components increases as  $\varepsilon_\Omega(< 0) \rightarrow 0$ , but the probability of  $\ell = 1$  components at  $\varepsilon_\Omega \Rightarrow 0$  is less than unity and depends on individual levels and deformations.

Except in very light nuclei a significant change of shell structure in weakly-bound protons is not expected because of the presence of the Coulomb barrier. For this reason the shell structure and magnetic moments of proton-drip-line nuclei are not included in this work. On the other hand, the magnetic moment of deformed odd- $Z$  nuclei towards the neutron drip line is a very useful and interesting quantity, since it may clearly show possible deformation of those nuclei. However, the proton separation energy of those neutron-rich nuclei is so large that the shell structure as well as magnetic moments can be reasonably evaluated using some old traditional models, for example, the modified-oscillator model. Therefore,

the numerical calculations are not included here.

When possible rotational spectra or strongly-enhanced quadrupole moments, which are the direct sign of deformation, are difficult to be measured in neutron drip line nuclei, an indication of deformation is to observe the unusually low-lying  $2^+$  state in even-even nuclei. On the other hand, one-particle motion in the mean field that shows the shape of nuclei can be easily recognized by studying the low-energy spectra of odd-A nuclei [8]. In particular, the spin-parity of low-lying states or magnetic moments of the ground or isomeric states of odd-A drip-line nuclei may be sometimes more easily measured and can be used as a clear indication of possible deformation. Therefore, in the present paper we survey the Nilsson diagrams that can be applicable to weakly-bound nuclei with  $N \approx 8, 20, 28$  and  $40$ , and give the estimated values of magnetic moments of possibly deformed odd-N nuclei with the neutron number close to those traditional magic numbers.

In section 2 the essential points of the model used in the present work are briefly summarized. Numerical examples for nuclei in the  $N \approx 8$  region is given in section 3.1, the  $N \approx 20$  region in section 3.2, the  $N \approx 28$  region in section 3.3, and the region  $N \approx 40$  region in section 3.4. Conclusions and discussions are given in section 4.

## II. MODEL

Recognizing the great usefulness of the Nilsson diagram, in which one-particle energies are plotted as a function of deformation parameter for a given potential, in the present article we apply the model and idea presented in [9]. The quadrupole deformation parameter  $\beta$  is defined in [10]. The coupled equations derived from the Schrödinger equation are solved in coordinate space with the correct asymptotic behaviour of wave functions for  $r \rightarrow \infty$ , both for bound [10] and resonant [11, 12] levels. In particular, one-particle resonant levels in a deformed potential are estimated using the eigenphase formalism [13]. Namely, one-particle resonance is obtained if one of calculated eigenphases increases through  $\pi/2$  as one-particle energy increases. One-particle resonance is not obtained if none of the calculated eigenphases increase through  $\pi/2$  as energy increases. The definition is a natural extension of the definition of one-particle resonance for spherical potentials in terms of phase shift, which can be found in standard textbooks. One-particle resonance with  $\Omega^\pi=1/2^+$  is not at all obtained if for  $\varepsilon_\Omega(< 0) \rightarrow 0$  the  $\ell=0$  component of the wave function inside the

potential exceeds a certain probability [12]. On the other hand, for  $\Omega^\pi \neq 1/2^+$  one-particle resonant levels can be always found at least for small positive energies. Compared with the Nilsson diagram based on modified oscillator potentials, the striking difference of the level scheme exhibited in the present work comes from the behaviour of levels with low  $\ell$  values (in particular,  $\ell=0$  and 1) for  $\beta=0$  and those with small  $\Omega$  values (in particular,  $\Omega^\pi = 1/2^+$ ,  $1/2^-$ , and  $3/2^-$ ) for  $\beta \neq 0$ , in both the weakly-bound and positive-energy regions.

We use the parameters of Woods-Saxon potentials taken from the standard ones [4] for stable nuclei except the depth,  $V_{WS}$ . The potential depth for neutrons is adjusted so that the energy of the one-neutron level last occupied in a given odd-N nucleus is close to the measured neutron separation energy. The diffuseness, the strength of the spin-orbit potential and the radius parameter are, for simplicity, taken from those on p.239 of [4]. Considering the possible contribution by weakly-bound neutron(s) to the self-consistent potential, a slightly larger diffuseness might be appropriate for presently studied nuclei. However, it is noted that the major part of the nuclear potential is provided by well-bound nucleons of the core. Moreover, a larger diffuseness leads to the degeneracy of the  $2s_{1/2}$  and  $1d_{5/2}$  ( $2p_{3/2}$  and  $1f_{7/2}$ ) levels already at a larger binding energy than the one exhibited in the present article. It is also remarked that for a given deformation the N-th deformed one-particle orbit filling-in all lower-lying Nilsson levels is almost uniquely determined for a given one-particle energy and within a reasonable variation of Woods-Saxon potential parameters.

The magnetic dipole moments of odd-N deformed nuclei are calculated using equations (4-86), (4-87), and (4-88) of [8], while the matrix elements of  $\ell_\nu$  and  $s_\nu$  are evaluated using one-particle wave-functions in the deformed Woods-Saxon potential. See equations (5-86) and (5-87) of [8]. The tabulated magnetic moments are calculated for the band-head states for given intrinsic configurations. The spin of the band-head state is  $I = \Omega$  for  $\Omega \neq 1/2$ . For  $\Omega=1/2$  configurations the decoupling parameter  $a$  is calculated, and the spin of the band-head state is different from  $I=1/2$  for both  $a < -1$  and  $a > 4$ . See [8].

The major part of the reduction of the effective  $g_s$  factor,  $g_s^{eff}$ , from  $g_s^{free}$  in the present model is supposed to come from the spin polarization of deformed even-even core. For large deformation where the asymptotic quantum numbers  $[N \ n_z \ \Lambda \ \Omega]$  become good quantum numbers, the spin polarizations of  $\Delta K=0$  type vanish, since the quantum numbers  $\Lambda$  and  $\Sigma (= \Omega - \Lambda)$  become constants of the motion. Consequently, the longitudinal  $g_s^{eff}$  factor may approach  $g_s^{free}$ , while the transverse matrix element  $(g_K - g_R)b$  in equation (4-86) of

[8] is still affected by the presence of  $\Delta K=1$  polarizations of deformed even-even core. The latter contributes only to the magnetic moments of  $K=1/2$  bands. The quenching of the spin fluctuations in the large deformation limit seems to be only partially achieved for the equilibrium deformations of stable deformed nuclei [14]. (A further reduction in the spin polarization of nuclei presently studied may come from the fact that loosely-bound neutrons couple weakly with strongly-bound core nucleons.) In the present numerical calculations we use  $g_s^{eff}=g_s^{free}$  in the lightest mass ( $N \approx 8$ ) region where deformed nuclei have larger deformation, while in heavier mass regions  $g_s^{eff}=(0.7)g_s^{free}$  is used. We do not try any detailed evaluation of the spin polarization effect in individual deformed nuclei, since our present aim is to show the spin-parity as well as magnetic moments for deformed shape of nuclei studied, which are very different from those for spherical shape.

In the present coupled channel calculation the  $j = 1/2, 3/2, 5/2, 7/2, 9/2, 11/2$  and  $13/2$  channels are included for positive-parity levels, while the  $j = 1/2, 3/2, 5/2, 7/2, 9/2$  and  $11/2$  channels for negative-parity levels.

### III. NUMERICAL EXAMPLES

#### A. Odd-N neutron-rich nuclei in $N \approx 8$ region

As it is known that the shape of the Be isotope can be very different for the A and A+1 nuclei, the notion of the mean field is not so well established in nuclei of this very light mass region. Nevertheless, in figure 2 the Nilsson diagram is shown, of which the parameters are adjusted to the nucleus  ${}^{17}_6\text{C}_{11}$ , since in this mass region the spin-parity and/or magnetic moments are measured for some odd-N nuclei with weakly-bound neutron(s). In figure 2 the  $[200\ 1/2]$  level can be obtained as a one-particle resonant level as far as  $d$  components are dominant. In contrast, for  $\beta > 0.46$  the resonant level is not obtained because the  $s$  component becomes dominant in the one-particle wave-function. Similarly, due to the  $s$ -component dominance the extension of the  $[220\ 1/2]$  level to the positive-energy region on the oblate side as a resonant level is not possible for  $\beta < -0.12$ .

In figure 2, it is seen that in the spherical limit ( $\beta=0$ ) the very weakly bound  $1d_{5/2}$  and  $2s_{1/2}$  levels are almost degenerate. Namely, as the binding becomes very weak, the energy eigenvalue of the  $s$  orbit shifts downward relative to that of the  $d$  level, as schematically

exhibited in figure 1. The calculated and measured magnetic moments of the ground state of  $^{17}_6\text{C}_{11}$  and  $^{11}_4\text{Be}_7$  are compared in table 1. It is remarked that for a much weaker strength of the potential such as the one applicable for  $^{11}\text{Be}$ , in which the  $[220\ 1/2]$  and  $[101\ 1/2]$  orbits at  $\beta \approx 0.6$  are bound by several hundreds keV, the calculated bound one-particle level scheme and magnetic moments around  $\beta=0.6$  are found to remain nearly the same. When in a given region of deformation the curve of the Nilsson level is almost a straight line as a function of deformation, the one-particle wave-function depends very little on deformation and, consequently, the calculated magnetic moment remains almost independent of deformation. We notice that measured magnetic moment of  $^{15}\text{C}_9$  ( $I=1/2^+$ ) that can be a spherical nucleus,  $|\mu| = 1.720 \pm 0.009 \mu_N$  [15], is nearly equal to that of  $^{11}\text{Be}_7$  ( $I^\pi=1/2^+$ ) that is most easily interpreted as a deformed nucleus, assuming that the sign of the former is minus. This is theoretically expected because the  $[220\ 1/2]$  wave-function of the 7th neutron in  $^{11}\text{Be}$  consists exclusively of  $1d_{5/2}$  and  $2s_{1/2}$  components, of which non-diagonal matrix element of magnetic dipole operator is zero, and, furthermore, the neutron one-particle magnetic moments of  $1d_{5/2}$  and  $2s_{1/2}$  are the same.

The spin-parity ( $3/2^+$ ) of the ground state of  $^{17}\text{C}_{11}$  is in a very natural way interpreted as the band-head state of the N=11th neutron occupying the  $[211\ 3/2]$  level. The near degeneracy of the  $1d_{5/2}$  and  $2s_{1/2}$  levels at  $\beta=0$  can well be the reason why the nucleus  $^{17}\text{C}$  is deformed (Jahn-Teller effect). The measured magnetic moment is in good agreement with the calculated value based on the deformation, as seen in table 1.

## B. Odd-N neutron-rich nuclei in $N \approx 20$ region

In figure 3 the Nilsson diagram is shown, of which the parameters are approximately adjusted to the nucleus  $^{31}_{10}\text{Ne}_{21}$ . For a slightly stronger potential which may be applicable for  $^{31}_{12}\text{Mg}_{19}$  (the neutron separation energy  $S_n = 2.38$  MeV) and  $^{33}_{12}\text{Mg}_{21}$  ( $S_n = 2.22$  MeV), the calculated bound one-particle level scheme and magnetic moments remain nearly the same as those presented here. See figure 3 of [9]. Neither the  $2p_{3/2}$  nor  $2p_{1/2}$  levels are obtained as one-particle resonant levels for the present potential. Nevertheless, in figure 3 the approximate positions of those levels, which are extrapolated from the resonance energies obtained for slightly stronger spherical Woods-Saxon potentials, are indicated in figure 3 with the question mark. It is noted that when both the  $2p_{3/2}$  and  $1f_{7/2}$  levels appear

as very low-lying resonant levels, the  $2p_{3/2}$  level may lie lower than the  $1f_{7/2}$  level.

The second lowest  $\Omega^\pi=1/2^-$  level for  $\beta > 0$  denoted by the dotted curve in figure 3 cannot continue for  $\beta < 0.33$  as a one-particle resonant level, because one-particle resonant levels with the major component of  $\ell=1$  cannot survive for higher  $\varepsilon_\Omega$  values. The complicated behaviour of the resonant level expressed by the dotted curve for  $\beta < 0$  indicates clearly the influence of the  $2p_{3/2}$  and  $2p_{1/2}$  levels that do not explicitly appear in figure 3. It is noted that for a pure  $1f_{7/2}$  shell the dotted curve increases almost linearly as  $|\beta|$  increases for  $\beta < 0$ , just as a smooth extension of the curve for  $\beta > 0$ . Around  $\beta = -0.4$  the major component of the  $\Omega^\pi=1/2^-$  level is  $\ell=1$ . As  $\beta(< 0)$  increases  $\varepsilon_\Omega$  increases, and the one-particle resonant level with the  $\ell=1$  major component can hardly survive for  $\varepsilon_\Omega > 1.2$  MeV, where both the width and  $\varepsilon_\Omega$  rapidly increase. The major component of the one-particle resonant level expressed by the dotted curve for  $-0.2 < \beta < 0.07$  is  $\ell=3$ , and consequently the resonant level is well defined with the reasonably small width.

The near degeneracy of  $1f_{7/2}$ ,  $2p_{3/2}$  and  $2p_{1/2}$  levels at  $\beta=0$  can be the origin of possible deformation that appears in the system with a few weakly bound neutrons occupying the  $1f_{7/2}$ - $2p_{3/2}$ - $2p_{1/2}$  shell (Jahn-Teller effect). Namely, using the degeneracy the energy of a particular combination of the  $pf$  components can be made lower when deformation sets in.

In this region of "island of inversion" there are two odd-N nuclei of which magnetic moments of the ground state are measured. The measured magnetic moment [18] of the ground state ( $I^\pi=1/2^+$ ) of  $^{31}_{12}\text{Mg}_{19}$  is  $-0.88355(15) \mu_N$ , while it is reported in [20] that the magnetic moment of  $^{33}_{12}\text{Mg}_{21}$  is  $-0.7456(5) \mu_N$  and the spin is  $3/2$ . Though the parity of the ground state of  $^{33}\text{Mg}$  is currently still under debate (for example, see the recent  $\beta$ -decay study in [19]), from table 2 the measured negative magnetic moment seems to have no other choice than negative parity for the ground state. It is remarked that the Nilsson orbit that can be occupied by the 21st neutron for  $0 < \beta \lesssim 0.6$  is either  $[330\ 1/2]$  or  $[202\ 3/2]$  or  $[321\ 3/2]$  within the reasonable variation of potential parameters. All of the three Nilsson orbits lead to  $I=3/2$  for the band-head spin. Considering that we have fixed parameters  $g_s^{eff}$  and  $g_R$  in the numerical calculation of magnetic moments, of which some standard values are used, the agreement of the calculated and measured values in table 2 is very good. In table 2 calculated magnetic moments are tabulated for a given  $\beta$  value, however, it should be noted that calculated values remain approximately constant, as far as the Nilsson level is almost a straight line as a function of  $\beta$ .



### C. Odd-N neutron-rich nuclei in $N \approx 28$ region

Odd-N nuclei with weakly bound neutrons in this region are currently under study and, to our knowledge, no measurements of magnetic moments are reported. Examining  $E(2_1^+)$  of even-even nuclei with  $N=28$ , possible candidates for the deformed ground state are  $^{42}_{14}\text{Si}_{28}$  and  $^{44}_{16}\text{S}_{28}$ , of which  $E(2_1^+)$  is 770 (19) [21] and 1297(18) keV [22], respectively. There have been both some shell-model calculation and more elaborated many-body calculation, which suggested an oblate deformation for the nucleus  $^{42}\text{Si}$ . Thus, in this region we show magnetic moments of odd-N nuclei evaluated for both prolate and oblate shape. Though  $^{40}\text{Mg}$  lies inside the neutron drip line, Mg isotope is not discussed here, since none of the neighboring odd-N nuclei,  $^{41}\text{Mg}$  and  $^{39}\text{Mg}$ , is bound.

In figure 4 we show the Nilsson diagram, of which the parameters are approximately adjusted to  $^{41}_{14}\text{Si}_{27}$ . The reported  $S_n$  value [23] of this nucleus is 1.34 MeV with a rather large ambiguity. It is seen that at  $\beta=0$  the  $2p_{3/2}$  level lies only 1.2 MeV higher than the  $1f_{7/2}$  level when the former is bound only by 0.28 MeV. Then, there may be a good chance for  $N=27$  nuclei being deformed, since the neutron number  $N=28$  may not work as a magic number.

Calculated magnetic moments are shown in table 3. It is interesting to see that the magnetic moment of  $^{41}\text{Si}$  can be very different if it has an oblate shape. This is because the (positive or) almost vanishing value of the calculated magnetic moment comes from a subtle balance between the  $p_{3/2}$  and  $p_{1/2}$  components in the one-particle wave-function of the  $[301\ 1/2]$  orbit. That means, the calculated magnetic moments of oblate nuclei with  $N=27$  depend on the size of the oblate deformation, as can be guessed from the curved (and not straight-line) Nilsson level in figure 4 as a function of  $\beta$ .

In the  $g$ -factor measurement of  $^{43}_{16}\text{S}_{27}$ , which is an isotone of  $^{41}\text{Si}$ , it is reported [24] that the 320 keV isomeric state has  $7/2^-$  and  $g=-0.317(4)$ . This observation of the excited state indicates that the ground state of  $^{43}\text{S}$  is deformed.

In figure 5 the Nilsson diagram for neutrons is shown, of which the parameters are approximately adjusted to  $^{45}_{16}\text{S}_{29}$ . The comparison between figure 4 and figure 5 clearly shows that the  $N=28$  shell-gap at  $\beta=0$ , namely the distance between the  $2p_{3/2}$  and  $1f_{7/2}$  levels, becomes increasingly smaller as the binding energy of the  $2p_{3/2}$  level approaches zero. This appreciable change of the  $N=28$  shell-gap indicates that for a given neutron-number  $N \approx 28$

the Si isotope has a better chance to be deformed than the S isotope. The nucleus  ${}^{43}_{14}\text{Si}_{29}$  is known to lie inside the neutron drip line, however, to our knowledge no spectroscopic information is yet available. In figure 5 the asymptotic quantum numbers,  $[N n_z \Lambda \Omega]$ , are written on the Nilsson levels which may be occupied by the N=29th neutron, while calculated magnetic moments, in which the last odd neutron is placed in respective Nilsson orbits, are given in table 4.

#### D. Odd-N neutron-rich nuclei in $N \approx 40$ region

Neutron-drip-line nuclei in the region of N=40 are still far away from reaching experimentally. Moreover, N=40 is not one of magic numbers in the j-j coupling shell model. Nevertheless, we include this subsection, because; (a) while there are no deformed N=40 nuclei along the stability line, recent experimental studies show relatively low energies ( $\approx 500$  keV) of the first excited 2+ state of even-even nuclei of both  ${}_{26}\text{Fe}$  and  ${}_{24}\text{Cr}$  isotopes in the region of  $N \approx 40$ . Indeed, it is stated [25] that the nucleus  ${}^{64}_{24}\text{Cr}_{40}$  may be a center of deformation in this region; (b) Some magnetic-moment measurements of isomeric states, the presence of which is not rare in this region, have already been reported.

Odd-N nuclei of Fe and Cr isotopes with  $N \approx 40$  around  ${}^{64}_{24}\text{Cr}_{40}$  have measured  $S_n$  values of a few MeV. In figure 6 the Nilsson diagram is shown, which may be useful for the Fe and Cr isotopes with  $N \approx 40$ . It is noted that the  $2p_{1/2}$  and  $1f_{5/2}$  levels in figure 6 are nearly degenerate in contrast to the level scheme shown in figures 4 and 5. This is because in the weaker potentials of the latter figures the  $2p_{1/2}$  level becomes increasingly lower relative to the  $1f_{5/2}$  level. Calculated magnetic moments are given in table 5, in which those given for  $\beta=0.25$  remain nearly the same for  $\beta=0.35$ . It may be speculated that the observed 387 keV isomeric state in  ${}^{67}_{26}\text{Fe}_{41}$  [26] may be the  $I^\pi=1/2^-$  or  $5/2^-$  state coming from the  $[301 1/2]$  or  $[303 5/2]$  intrinsic configuration if the isomeric state is deformed.

## IV. CONCLUSIONS AND DISCUSSIONS

Examples of the change of neutron shell-structure for weakly bound neutrons are illustrated for neutron-rich nuclei with  $N \approx 8, 20, 28$  and  $40$ . Both weakly-bound and resonant one-particle levels are properly calculated by directly solving the Schrödinger equation in

mesh of space coordinate with the appropriate boundary condition. Magnetic moments of possibly deformed odd-N nuclei in the region are calculated using one-particle wave-functions in deformed Woods-Saxon potentials.

Among the examples taken in the present paper, the near degeneracy of the weakly-bound  $1d_{5/2}$  and  $2s_{1/2}$  levels (figure 2), that of the one-particle resonant  $1f_{7/2}$ ,  $2p_{3/2}$  and  $2p_{1/2}$  levels (figure 3), and that of the  $1f_{5/2}$  and  $2p_{1/2}$  levels bound by several MeV (figure 6) are the most clear-cut examples of the unique shell-structure, which is very different from what is known for traditional stable nuclei. It is hoped that more experiments will pin down the unique shell structure. In the present paper we have argued that the shell structure may lead to, among others; (a) the appearance of the N=16 magic number [27]; (b) possible deformed shapes of  $^{11-14}\text{Be}$  [28],  $^{17}\text{C}$ , and  $^{19}\text{C}$ ; (c) deformed nuclei in the island of inversion around N  $\approx 20$ ; (d) The disappearance of the magic number N=28 and possible deformation of some neutron-drip-line nuclei with N $\approx 28$ .

Calculated magnetic moments of the deformed ground states of  $^{11}\text{Be}$ ,  $^{17}\text{C}$ ,  $^{31}\text{Mg}$ , and  $^{33}\text{Mg}$  are in good agreement with already measured ones, while the values of  $g_s$  and  $g_R$  have not been adjusted to individual nuclei. Except the case of  $^{11}\text{Be}$  where the unique magnetic moments of the  $d_{5/2}$ - $s_{1/2}$  mixed neutron wave-functions play a role, both measured and calculated values of magnetic moment are significantly different from what is expected from spherical shape and, thus, can be used as a good identification of deformation. The measurement of magnetic moments of other neutron-drip-line nuclei is strongly wanted.

Magnetic moments estimated in the present work are applicable not only to the ground state of the odd-N nuclei studied but also to excited or isomeric states in the neighboring nuclei. The presence of isomeric states is often expected in the region of N $\approx 28$  and N $\approx 40$  neutron-rich nuclei due to the coexistence of spherical and deformed shape or the unique shell-structure. Magnetic moments presently estimated for a given deformation remain nearly the same when one-particle energies in the Nilsson diagram vary almost linearly as a function of deformation, because the structure of single-particle wave-functions in those cases remains nearly independent of deformation.

It should be remarked that the change of the shell structure described in the present paper is different from (and independent of) the one coming from the neutron-proton tensor force [29], which is currently very fashionable for being an origin of shell-structure change. The latter depends on the proton number of respective nuclei when the neutron shell-structure

is discussed. Moreover, the effect of the tensor force is usually estimated using harmonic oscillator wave-functions in the shell model and, thus, the effect of weakly binding is not included.

The author is grateful to Dr. H. Ueno for introducing measured magnetic moments of neutron-rich nuclei in the presently-studied mass region to her.

- 
- [1] Klapisch R, Thibault-Philippe C, Detraz C, Chaumont J, Bernas R and Beck E 1969 *Phys. Rev. Lett.* **23** 652
  - [2] Thibault C, Klapisch R, Rigaud C, Poskanzer A M, Prieels R, Lessard L and Reisdorf W 1975 *Phys. Rev. C* **12** 644
  - [3] Warburton E K, Becker J A and Brown B A 1990 *Phys. Rev. C* **41** 1147
  - [4] Bohr A and Mottelson B R 1969 *Nuclear Structure* vol 1 (Massachusetts: Benjamin)
  - [5] Hamamoto I and Mottelson B R 2003 *C. R. Phys.* **4** 433
  - [6] Hamamoto I 2007 *Eur. Phys. J. Special Topics* **150** 123
  - [7] Suzuki D *et al* 2009 *Phys. Rev. Lett.* **103** 152503
  - [8] Bohr A and Mottelson B R 1975 *Nuclear Structure* vol 2 (Massachusetts: Benjamin)
  - [9] Hamamoto I 2007 *Phys. Rev. C* **76** 054319
  - [10] Hamamoto I 2004 *Phys. Rev. C* **69** 041306(R)
  - [11] Hamamoto I 2005 *Phys. Rev. C* **72** 024301
  - [12] Hamamoto I 2006 *Phys. Rev. C* **73** 064308
  - [13] For example, see; Newton R G 1966 *Scattering Theory of Waves and Particles* (New York: McGraw-Hill)
  - [14] Bodenstedt E and Rogers J D 1964 *in Perturbed Angular Correlations* (Amsterdam: North-Holland) eds Karlsson E, Matthias E and Siegbahn K
  - [15] Asahi K *et al* 2002 *Nucl. Phys.* **A704** 88c
  - [16] Ueno H *et al* 2004 *Nucl. Phys.* **A738** 211
  - [17] Geithner W 1999 *Phys. Rev. Lett.* **83** 3792

- [18] Neyens G *et al* 2005 *Phys. Rev. Lett.* **94** 022501
- [19] Tripathi V *et al* 2008 *Phys. Rev. Lett.* **101** 142504
- [20] Yordanov D T *et al* 2007 *Phys. Rev. Lett.* **99** 212501
- [21] Bastin B *et al* 2007 *Phys. Rev. Lett.* **99** 022503
- [22] Glasmacher T *et al* 1997 *Phys. Lett.* **B395** 163
- [23] Jurado B *et al* 2007 *Phys. Lett.* **B649** 43
- [24] Gaudefroy L *et al* 2009 *Phys. Rev. Lett.* **102** 092501
- [25] Adrich P *et al* 2008 *Phys. Rev. C* **77** 054306
- [26] Sawicka M *et al* 2003 *Eur. Phys. J. A* **16** 51
- [27] Ozawa A, Kobayashi T, Suzuki T, Yoshida K and Tanihata I 2000 *Phys. Rev. Lett.* **84** 5493
- [28] Hamamoto I and Shimoura S 2007 *J. of Phys.* **G34** 2715
- [29] For example, see; Otsuka T, Suzuki T, Fujimoto R, Grawe H, and Akakishi Y 2005 *Phys. Rev. Lett.* **95** 232502

TABLE I: Calculated magnetic dipole moments of the ground states of very light odd-N nuclei with one weakly-bound neutron, in comparison with observed ones. Measured neutron separation energies are expressed by  $S_n$ . Values of  $g_R=0.35$  (for  $\beta \neq 0$ ) and  $g_s^{eff}=g_s^{free}$  are used. Corresponding one-particle levels in figure 2 are those labeled as  $[211\ 3/2]$ ,  $[220\ 1/2]$  and  $2s_{1/2}$  for  $^{17}\text{C}$ ,  $^{11}\text{Be}$  and  $^{15}\text{C}$ , respectively.

Nucleus	$S_n$ (keV)	$I^\pi$	$\mu_{obs}$ ( $\mu_N$ )	Reference	$\mu_{calc}$ (at $\beta$ , [N n <sub>z</sub> $\Lambda$ $\Omega$ ]) ( $\mu_N$ )
$^{17}\text{C}_{11}$	727	$3/2^+$	$\pm 0.758(4)$	[16]	$-0.75$ ( $\beta=0.4$ , $[211\ 3/2]$ )
$^{11}\text{Be}_7$	504	$1/2^+$	$-1.6816(8)$	[17]	$-1.7$ ( $\beta=0.6$ , $[220\ 1/2]$ )
$^{15}\text{C}_9$	1218	$1/2^+$	$\pm 1.720(9)$	[15]	$-1.9$ ( $\beta=0$ , $2s_{1/2}$ )

TABLE II: Calculated magnetic dipole moments of N=21 and 19 nuclei, in which the last odd neutron is placed in corresponding Nilsson orbits for prolate shape, in comparison with available experimental data. See the Nilsson diagram in figure 3. Values of  $g_R=0.38$  and  $g_s^{eff} = (0.7)g_s^{free}$  are used. Note that for spherical shape one obtains  $\mu_{calc}(f_{7/2}) = -1.3\ \mu_N$  and  $\mu_{calc}(d_{3/2}) = +0.80\ \mu_N$ , respectively, using  $g_s^{eff} = (0.7)g_s^{free}$ .

Nucleus	$S_n$ (keV)	$(I^\pi)_{obs}$	$\mu_{obs}$ ( $\mu_N$ )	Reference	$(I^\pi)_{cal}$	$\mu_{calc}$ (at $\beta$ , [N n <sub>z</sub> $\Lambda$ $\Omega$ ]) ( $\mu_N$ )
$^{33}\text{Mg}_{21}$	2222	$3/2$	$-0.7456(5)$	[20]	$3/2^-$	$-0.88$ ( $\beta=0.25$ , $[330\ 1/2]$ )
					$3/2^+$	$+0.91$ ( $\beta=0.35$ , $[202\ 3/2]$ )
					$3/2^-$	$-0.39$ ( $\beta=0.45$ , $[321\ 3/2]$ )
$^{31}\text{Mg}_{19}$	2378	$1/2^+$	$-0.88355(15)$	[18]	$1/2^+$	$-1.00$ ( $\beta=0.45$ , $[200\ 1/2]$ )
					$3/2^-$	$-0.91$ ( $\beta=0.35$ , $[330\ 1/2]$ )

TABLE III: Calculated magnetic dipole moments of N=27 nuclei, in which the last odd neutron is placed in corresponding Nilsson orbits. See the Nilsson diagram in figure 4. Values of  $g_R=0.38$  and  $g_s^{eff} = (0.7)g_s^{free}$  are used. Note that for spherical shape one obtains  $\mu_{calc}(p_{1/2}) = +0.4 \mu_N$ ,  $\mu_{calc}(p_{3/2}) = -1.3 \mu_N$  and  $\mu_{calc}(f_{7/2}) = -1.3 \mu_N$ , respectively, using  $g_s^{eff} = (0.7)g_s^{free}$ .

Nucleus	$S_n$	$(I^\pi)_{cal}$	$\mu_{calc}$ (at $\beta$ , [N n <sub>z</sub> $\Lambda$ $\Omega$ ])
	(MeV)		( $\mu_N$ )
<sup>41</sup> Si <sub>27</sub>	1.34	3/2 <sup>-</sup>	+0.07 ( $\beta=-0.4$ , [301 1/2])
		3/2 <sup>-</sup>	-0.66 ( $\beta=0.25$ , [321 1/2])
		5/2 <sup>-</sup>	-0.58 ( $\beta=0.45$ , [312 5/2])

TABLE IV: Calculated magnetic dipole moments of N=29 nuclei, in which the last odd neutron is placed in corresponding Nilsson orbits. See the Nilsson diagram in figure 5. Values of  $g_R=0.38$  and  $g_s^{eff} = (0.7)g_s^{free}$  are used. Note that for spherical shape one obtains  $\mu_{calc}(p_{1/2}) = +0.4 \mu_N$ ,  $\mu_{calc}(p_{3/2}) = -1.3 \mu_N$  and  $\mu_{calc}(f_{7/2}) = -1.3 \mu_N$ , respectively, using  $g_s^{eff} = (0.7)g_s^{free}$ .

Nucleus	$S_n$	$(I^\pi)_{cal}$	$\mu_{calc}$ (at $\beta$ , [N n <sub>z</sub> $\Lambda$ $\Omega$ ])
	(MeV)		( $\mu_N$ )
<sup>45</sup> S <sub>29</sub>	2.21	7/2 <sup>-</sup>	-0.74 ( $\beta = 0.25$ , [303 7/2])
		1/2 <sup>-</sup>	+0.59 ( $\beta=0.45$ , [310 1/2])
		1/2 <sup>-</sup>	+0.59 ( $\beta=-0.40$ , [310 1/2])
		3/2 <sup>-</sup>	+0.16 ( $\beta=-0.40$ , [312 3/2])

TABLE V: Calculated magnetic dipole moments of  $N \approx 40$  nuclei, in which the last odd neutron is placed in corresponding Nilsson orbits. See the Nilsson diagram in figure 6. Values of  $g_R=0.38$  and  $g_s^{eff} = (0.7)g_s^{free}$  are used. Note that for spherical shape one obtains  $\mu_{calc}(p_{1/2}) = +0.4 \mu_N$ ,  $\mu_{calc}(f_{5/2}) = +1.0 \mu_N$  and  $\mu_{calc}(g_{9/2}) = -1.3 \mu_N$ , respectively, using  $g_s^{eff} = (0.7)g_s^{free}$ .

Nilsson orbits ([N n <sub>z</sub> $\Lambda$ $\Omega$ ])	$\beta$	$(I^\pi)_{cal}$	$\mu_{calc}$ ( $\mu_N$ )
([303 5/2])	0.25	5/2 <sup>-</sup>	+1.1
([301 1/2])	0.25	1/2 <sup>-</sup>	+0.43
([431 3/2])	0.25	3/2 <sup>+</sup>	-0.19
([422 5/2])	0.35	5/2 <sup>+</sup>	-0.46
([301 3/2])	0.35	3/2 <sup>-</sup>	-0.40

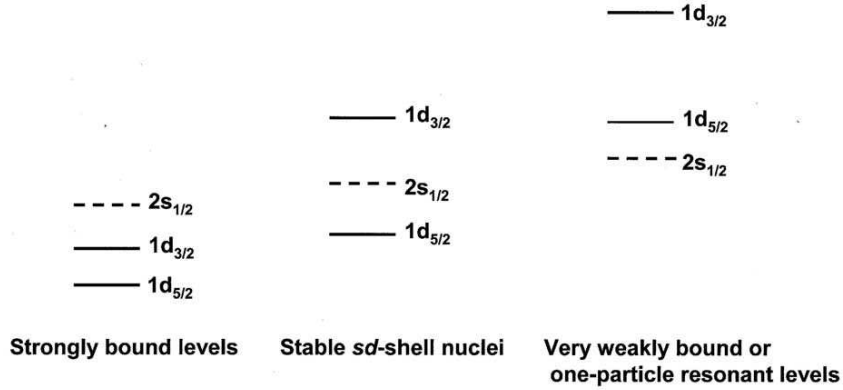


FIG. 1: Qualitative sketch of relative energies of three one-neutron levels in the  $sd$  shell depending on the binding energy or the potential strength. The level order sketched in the middle figure is the one known from stable  $sd$  shell nuclei.





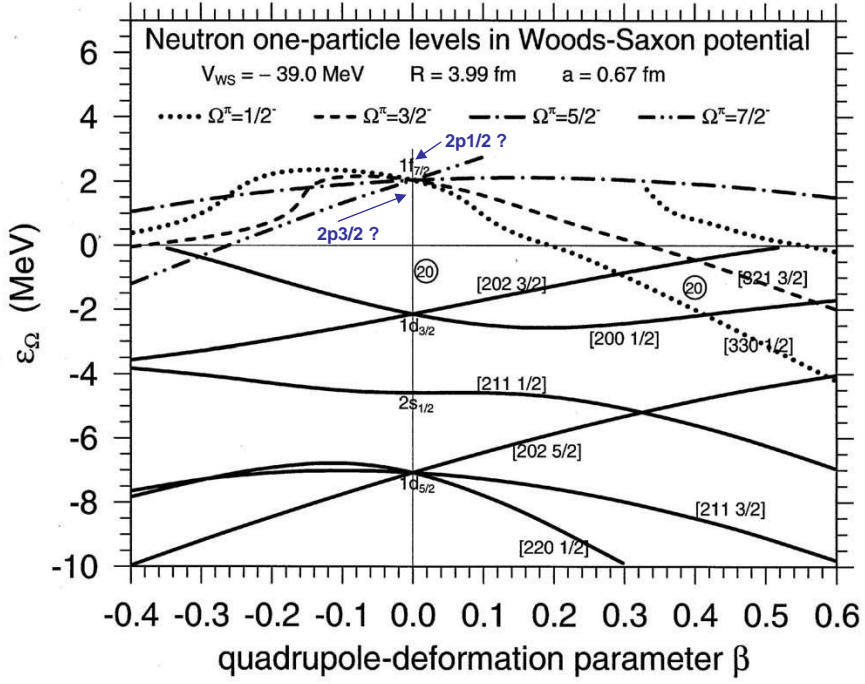


FIG. 3: Neutron one-particle levels as a function of axially-symmetric quadrupole deformation. Parameters of the Woods-Saxon potential are designed approximately for the nucleus  ${}^{31}_{10}\text{Ne}_{21}$ , of which the measured  $S_n$  value is  $(0.3 \pm 1.6)$  MeV. The diffuseness, the radius and the depth of the Woods-Saxon potential are 0.67 fm, 3.99 fm, and  $-39.0$  MeV, respectively. Some one-particle levels are denoted by the asymptotic quantum numbers,  $[Nn_z\Lambda\Omega]$ . Positive-parity levels are plotted by solid curves. The neutron number 20, which is obtained by filling in all lower-lying levels, is indicated with a circle. The  $2p_{3/2}$  and  $2p_{1/2}$  neutron levels at  $\beta=0$  are not obtained as one-particle resonant levels, and the next low-lying one-particle resonant level at  $\beta=0$  is the  $1f_{5/2}$  level found at 9.50 MeV. The approximate positions of the  $2p_{3/2}$  and  $2p_{1/2}$  levels at  $\beta=0$  are indicated with "?", which are extrapolated from the resonant energies obtained by using a slightly stronger Woods-Saxon potential. See the text for details.

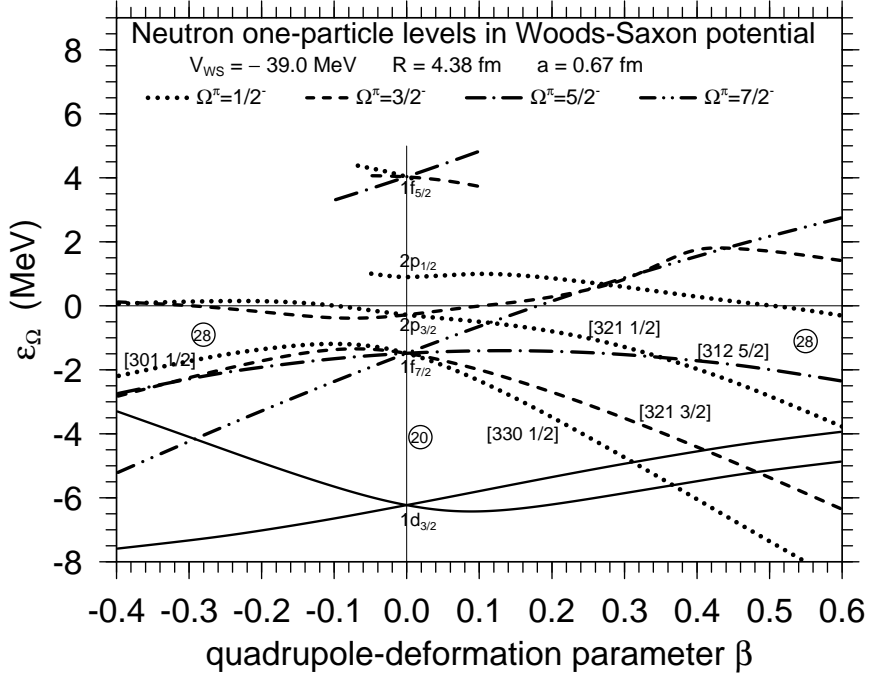


FIG. 4: Neutron one-particle levels as a function of axially-symmetric quadrupole deformation. Parameters of the Woods-Saxon potential are designed approximately for the nucleus  ${}^{41}_{14}\text{Si}_{27}$ , of which  $S_n = 1.34$  MeV. The diffuseness, the radius and the depth of the Woods-Saxon potential are 0.67 fm, 4.38 fm, and  $-39.0$  MeV, respectively. Some one-particle levels are denoted by the asymptotic quantum numbers,  $[Nn_z\Lambda\Omega]$ . Positive-parity levels are plotted by solid curves. The neutron numbers 20 and 28, which are obtained by filling in all lower-lying levels, are indicated with circles. The  $\Omega^\pi=1/2^-$  level originating from  $2p_{1/2}$  at  $\beta=0$  does not survive as one-particle resonance for  $\varepsilon_\Omega > 1$  MeV and  $\beta < -0.05$ . On the other hand, for simplicity of the figure, only in the neighborhood of  $\beta=0$  we have plotted resonant levels originating from  $f_{5/2}$ . See the text for details.

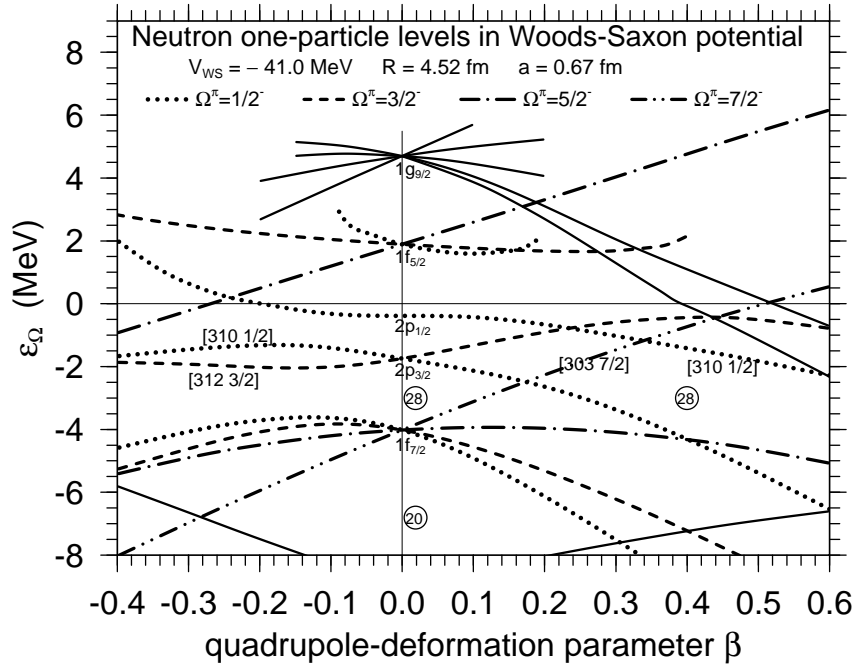


FIG. 5: Neutron one-particle levels as a function of axially-symmetric quadrupole deformation. Parameters of the Woods-Saxon potential are designed approximately for the nucleus  ${}^{45}_{16}\text{S}_{29}$ , of which  $S_n = 2.21$  MeV. The diffuseness, the radius and the depth of the Woods-Saxon potential are 0.67 fm, 4.52 fm, and  $-41.0$  MeV, respectively. Some one-particle levels possibly occupied by the N=29th neutron are denoted by the asymptotic quantum numbers,  $[Nn_z\Lambda\Omega]$ . Positive-parity levels are plotted by solid curves. The neutron numbers 20 and 28, which are obtained by filling in all lower-lying levels, are indicated with circles. Neutron resonant levels originating from  $1f_{5/2}$  at  $\beta=0$  are plotted as far as they are obtained following the definition of the eigenphase formalism. On the other hand, not all neutron resonant levels originating from  $1g_{9/2}$  are plotted, for simplicity of the figure. See the text for details.

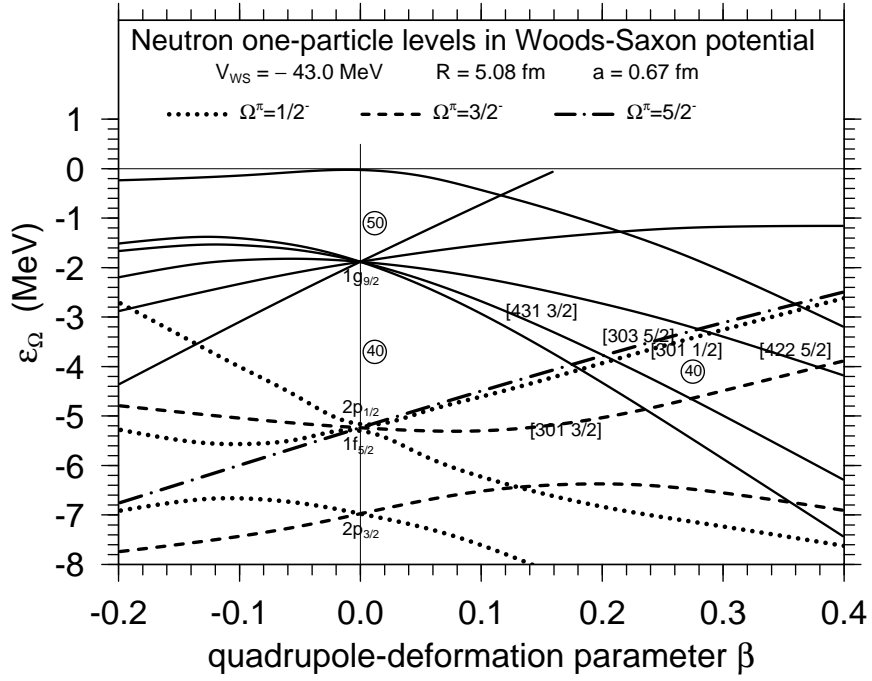


FIG. 6: Neutron one-particle levels as a function of axially-symmetric quadrupole deformation. Parameters of the Woods-Saxon potential are designed approximately for the nucleus  ${}^{65}_{26}\text{Fe}_{39}$ , of which  $S_n = 4.18$  MeV. The diffuseness, the radius and the depth of the Woods-Saxon potential are 0.67 fm, 5.08 fm, and  $-43.0$  MeV, respectively. Some one-particle levels possibly occupied by the  $N \approx 40$ th neutron for some prolate deformation are denoted by the asymptotic quantum numbers,  $[N n_z \Lambda \Omega]$ . Positive-parity levels are plotted by solid curves. The neutron numbers 40 and 50, which are obtained by filling in all lower-lying levels, are indicated with circles. See the text for details.